Research Letter **DOI:** 10.15541/jim20250017

Colorless/Black Switching Electrochromic Device Based on $WO_3 \cdot xH_2O$ and Reversible Metal Electrodeposition

WAN Xinyi[1], WANG Wenqi[1], LI Jiacheng[1], ZHAO Junliang[2], MA Dongyun[1], WANG Jinmin[1]

(1. School of Materials and Chemistry, University of Shanghai for Science and Technology, Shanghai 200093, China; 2. Shanghai Berma Enterprise Development Group Co., Ltd., Shanghai 201306, China)

Abstract: Electrochromic (EC) smart windows utilizing a reversible metal electrodeposition device (RMED) offer a compelling alternative for dynamically regulating transmissions of optical and thermal energy. An EC device (ECD) is constructed by reversible metal electrodeposition (RME) of Bi/Cu on $WO_3 \cdot xH_2O$ film electrodeposited onto fluorine-doped tin oxide (FTO) transparent conductive glass. The electrolyte consists of $CuCl_2$, $BiCl_3$, KCl and HCl aqueous solution, supplying necessary components for both electrochemical and electrodeposition processes. The ECD shows ability to rapidly transition between colorless and black states, which achieves a large optical modulation of 77.0% at 570 nm. In the black state, the ECD exhibits a near-zero transmittance in the wavelength range of 400–1100 nm while maintaining 96.6% of its initial optical modulation after coloration/bleaching cycling of 60000 s, exhibiting good cyclic stability. This RMED has relatively high stability under open-circuit voltage and also possesses excellent heat insulation performance. The results offer a solution to overcome the poor cyclic stability of RMEDs and improve the optical modulation of ECDs.

Key words: reversible metal electrodeposition; electrochromic; $WO_3 \cdot xH_2O$

In recent years, energy efficiency has been crucial. Building heating, ventilation and air conditioning (HVAC) consumes 40% of global energy. Smart windows can cut 20% of energy use in buildings[1-4]. EC materials or devices reversibly control their coloration and bleaching states by applying a voltage bias[5-6]. Despite decades of research, conventional ECDs have not yet been widely adopted due to issues such as difficulty in achieving transparency to black, high cost, slow switching speed and durability[7-8]. Recently, RMEDs have emerged as promising ECDs. It offers impressive spectral modulation capabilities in both visible and infrared regions. RMED has a simple structure, low energy consumption, and the ability to modulate multiple color states. These features make it highly suitable for applications in smart windows, thermal management, and information display[9-16]. Similar to other traditional color-changing smart windows, color-changing process of RMED is accompanied by a redox reaction, which corresponds to the process of dissolution (bleaching) or deposition (coloration) of metals[17-20]. Unlike conventional color-changing devices, RMED does not have an EC layer. The entire RMED is operated under different external biases, and under the condition of applying a reduction voltage, metal ions are deposited to the working electrode (the device is changed from a bleached state to a colored state). By applying an oxidation voltage, the metal is dissolved and transforms into ions that return to the electrolyte (the device is changed from a colored state to a bleached state)[21-23]. The colored state of other ECDs can achieve very low transmittance in a specific wavelength range, whereas the colored state of RMED can achieve nearly zero transmittance across the entire wavelength spectra[24-26]. However, these devices also have drawbacks. The bleaching voltage needs to be lower than the metal ion deposition voltage. Otherwise, reverse coloration will occur. Moreover, the deposited metal will gradually dissolve without an applied voltage, and a certain voltage must be continuously applied to maintain the coloration of the device, resulting in poor steady-state performance. Previous research efforts have identified some methods

Received date: 2025-01-13; **Revised date:** 2025-03-03; **Published online:** 2025-04-09
Biography: 宛心怡(2000–), 女, 硕士研究生. E-mail: 222143048@st.usst.edu.cn
WAN Xinyi (2000–), female, Master candidate. E-mail: 222143048@st.usst.edu.cn
Corresponding author: 王金敏, 教授. E-mail: jmwang@usst.edu.cn.
WANG Jinmin, professor. E-mail: jmwang@usst.edu.cn.

to enhance the device's steady state. However, as the steady state of the device increases, generally, bleaching becomes more difficult, which means that the required bleaching voltage will rise and may exceed the metal ion deposition voltage[27-29].

Prior research has demonstrated that widely employed cathode-coloring materials have superior optical modulation and longer durability in comparison with that of anode-coloring materials[30]. The objective is to incorporate cathode-coloring EC materials into metal electrodeposition in order to create ECDs that exhibit enhanced performance. Tungsten oxide (WO_3) is a well-researched inorganic anode-coloring EC material known for its exceptional characteristics, including rapid coloration and bleaching response, significant optical modulation, and reliable cyclic stability[31-32]. Currently, Cu^{2+} and Bi^{3+} are the primary metal ions used in RME electrolytes for dynamic RME windows due to their affordability and favorable standard reduction potential. Islam *et al*.[33] conducted an in-depth study on the reversible Bi/Cu electrodeposition system. They fabricated a dynamic window with rapid switching capability, color neutrality, durable cycling performance, and bistable static stability. Nguyen *et al*.[27] managed to modify the surface of the transparent conductive electrode (TCE) with amorphous WO_3, subsequently developing a RME window based on the Bi/Cu system. The presence of WO_3 as an electrode shielding layer on the TCE surface played a crucial part, leading to a substantial enhancement in the device's durability. However, the optical modulation of the device is not high.

In this study, an RMED based on Cu/Bi metal electrodeposition on hydrated tungsten oxide ($WO_3{\cdot}xH_2O$) film is developed, which can be reversibly switched between black and colorless states. The transmittance of the colored device is less than 0.04%, achieving complete optical-blocking effect. Additionally, the device has a relatively large optical modulation in both visible and near-infrared regions, fast responses and good cyclic stability.

1 Experimental

1.1 Materials

The chemicals used in the study were not subjected to additional purification. Anhydrous ethanol (C_2H_5OH, 98%), sodium tungstate dihydrate ($Na_2WO_4{\cdot}2H_2O$, 98%), hydrogen peroxide (H_2O_2, 30%), nitric acid (HNO_3, 65%–68%), potassium chloride (KCl, 99.5%), bismuth trichloride ($BiCl_3$, 99.9%), copper chloride dihydrate ($CuCl_2{\cdot}2H_2O$, 99.0%), hydrochloric acid (HCl, 36%–38%) were obtained from Shanghai Titan Scientific Co., Ltd. (China). Fluorine-doped tin oxide (FTO) transparent conductive glasses with a square resistance of less than 15 $\Omega{\cdot}\square^{-1}$ and an optical transmittance of over 83% were acquired from Zhuhai Kaivo Optoelectronic Technology Co., Ltd. (China).

1.2 Preparation of electrolyte

The electrolyte was prepared as follows: 0.225 g of $CuCl_2{\cdot}2H_2O$, 0.158 g of $BiCl_3$ and 7.45 g of KCl were dissolved in 100 mL of deionized water while swirling with a magnetic stirrer. Subsequently, 0.4 mL of HCl was introduced and agitated at room temperature for 20 min.

1.3 Preparation of $WO_3{\cdot}xH_2O$ film

The $WO_3{\cdot}xH_2O$ film was fabricated using constant voltage electrodeposition mode[32]. The working electrode was subjected to a constant voltage of –0.7 V for 400 s. The preparation of the deposition solution was carried out in the following manner. A solution was prepared by dissolving 1.65 g of $Na_2WO_4{\cdot}2H_2O$, 0.6 mL of H_2O_2, and 1.6 mL of HNO_3 in 200 mL of deionized water. The solution was agitated for 1 h at room temperature and then left to age for a week before being used. The FTO glasses (25 mm×50 mm) were sequentially cleaned using ethanol and deionized water. The process of electrodeposition was conducted using a three-electrode system. In this system, the working electrode was FTO glass, the counter electrode was Pt sheet, and the reference electrode was Ag/AgCl electrode.

1.4 Fabrication of ECD

The ECD is composed of three components: blank FTO glass, liquid electrolyte, and FTO glass coated with the $WO_3{\cdot}xH_2O$ film. Two pieces of FTO glass, one with the $WO_3{\cdot}xH_2O$ film, are joined together using transparent double-sided adhesives with 1 mm of thickness. Subsequently, the electrolyte is introduced into the device *via* a syringe. A device with a 15 mm×30 mm active area was used.

1.5 Characterization

The phase identifications of the Bi/Cu films electrodeposited on the $WO_3{\cdot}xH_2O$ film were determined using grazing incidence X-ray diffractometer (GIXRD, Rigaku Smartlab 3 kW, Japan) at an incidence angle of 0.5°. The film morphology was analyzed using a scanning electron microscope (SEM, ZEISS Gemini 300, German). The cyclic voltammetry (CV) curves of the films were obtained using an electrochemical workstation (CHI 760E, China) equipped with a three-electrode setup. The working electrode, counter electrode, and reference electrode in the Cu/Bi liquid electrolyte are FTO glass deposited with the $WO_3{\cdot}xH_2O$ film, Pt sheet and Ag/AgCl electrode, respectively. The ultraviolet-visible spectrophotometer (UH5700, HITACHI, Japan) was used to measure the transmission spectra of the ECD before and after switching. The measurements were taken over a wavelength range from 400 to 1100 nm.

2　Results and discussion

2.1　Mechanism analysis of Bi/Cu based RMEDs

Fig. 1(a, b) illustrate randomly distributed Bi^{3+} (yellow balls) and Cu^{2+} (purple balls) ions in the electrolyte in the absence of applied voltage. At –3.0 V for 30 s, Bi^{3+} and Cu^{2+} ions get electrons and can be electrodeposited onto the $WO_3 \cdot xH_2O$ film forming a black bimetallic film. At the same time, the $WO_3 \cdot xH_2O$ film will also change from colorless to blue. The commonly used cathode-coloring EC material $WO_3 \cdot xH_2O$, has large optical modulation and long cycle life. Additionally, it has a coarse texture that facilitates the process of metal electrodeposition, which accelerates the rate of metal electrodeposition. The black metallic film and the colored $WO_3 \cdot xH_2O$ film result in very low transmittance of the Bi/Cu based RMED. At an oxidation bias, the black film is oxidized to Bi^{3+} and Cu^{2+} ions, causing the film to dissolve back into the electrolyte and the device returns to a transparent colorless state (Fig. 1(c, d)).

As shown in Fig. 2, Cu firstly loses an electron to become Cu^+ ions, then a portion of Cu^+ ions lose an electron to become Cu^{2+} ions back to the electrolyte. Another part of Cu^+ ions undergoes a substitution reaction with Bi^{3+} ions, and a small amount of CuCl is formed. The mechanism of EC processes in the $WO_3 \cdot xH_2O$ film is as follows:

$$WO_3 \cdot xH_2O + ye^- + yH^+ \leftrightarrow H_yWO_3 \cdot xH_2O \quad (1)$$

When a voltage of –3.0 V is applied to the working electrode, the $WO_3 \cdot xH_2O$ film is colored and metal can be uniformly deposited on the $WO_3 \cdot xH_2O$ film (Fig. 3(a)). When a positive voltage is applied to the working electrode, the $WO_3 \cdot xH_2O$ film is oxidized. Response time tests were conducted on the RMED with electrolytes of various Cu/Bi atomic ratios, as depicted in Fig. S1. The results indicate that a Cu/Bi atomic ratio of 3 : 1 leads to the fastest stripping speed. This competing pathway in the stripping mechanism explains why stripping kinetics require an optimal atomic ratio of Cu to Bi of 1 : 3. When the proportion of Cu to Bi is at a relatively low level, the substitution reaction of Cu for Bi proceeds sluggishly. This is due to the insufficient amount of Cu available to displace the surplus Bi present on the surface. Conversely, if the atomic ratio of Cu to Bi within the electrodeposits is rather high, the elevated concentration of Cu^+ ions leads to the formation of insoluble CuCl, as shown in Fig. 3(b). This occurrence detrimentally affects the overall kinetics of the stripping process, causing it to decelerate. The formation of CuCl restricts the mobility

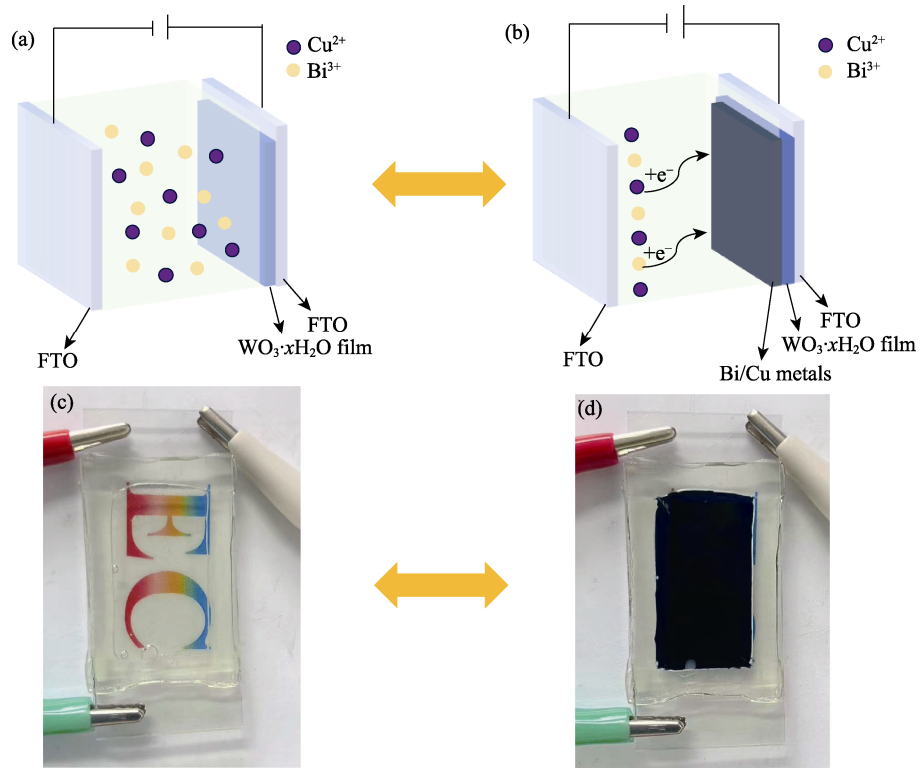

Fig. 1　Schematic illustration and photos of the RMED

(a, b) Schematic diagrams of the RMED in the (a) bleached state and (b) colored state; (c, d) Photos of the RMED (c) after 40 s of metal stripping at 1.0 V and (d) after 30 s of metal electrodeposition at –3.0 V

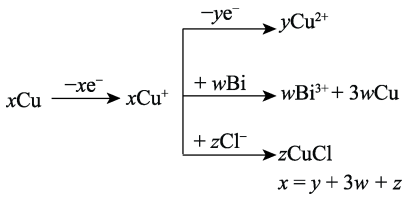

Fig. 2 Mechanism of stripping reactions in the Bi/Cu halide electrolyte

and reactivity of the relevant ions, impeding the efficient progress of the stripping reaction. As the atomic ratio of Cu to Bi rises, the substitution reaction rate is enhanced. This has significant implications for the optimization of the electrodeposition process and the overall performance of the resulting materials in various applications, such as in ECD where the precise control of the deposition composition is crucial for achieving desired optical and electrical properties[34].

2.2 Structure and morphology of the Cu and Bi metal films and the $WO_3 \cdot xH_2O$ film

Fig. 4 shows the GIXRD patterns of the Cu and Bi films electrodeposited on the $WO_3 \cdot xH_2O$ film. The $WO_3 \cdot xH_2O$ film shows an amorphous structure. Therefore, the obvious diffraction peaks in Fig. 4 suggest that Cu/Bi are successfully electrodeposited on the $WO_3 \cdot xH_2O$ film. The sharp peaks indicate that the films electrodeposited on the substrate are highly crystalline. The peaks at 2θ=28.4°, 32.1°, 66.7° are assigned to the monoclinic structure of Bi_2O_3 (JCPDS card No. 18-0244). The peaks at 2θ=43.2°, 50.4°, 74.1° are assigned to the monoclinic structure of Cu (JCPDS card No. 04-0836). The results are in good agreement with previous reports of cubic Cu[35-36].

The morphological and microstructural characteristics of the $WO_3 \cdot xH_2O$ film, as well as the Cu/Bi film electrodeposited onto it, were thoroughly investigated using the SEM technique. In Fig. 5(a), the $WO_3 \cdot xH_2O$ film deposited on the FTO glass exhibits a remarkably even surface and a highly compact structure. This specific microstructure is a direct consequence of the intricate processes involved in the formation and subsequent growth of crystal nuclei. The rough surface texture is a result of the underlying crystalline arrangement, which offers a conducive environment for the deposition of metal. This roughness provides numerous nucleation sites, facilitating the adhesion and growth of metal atoms during the electrodeposition process. The uniformity of the $WO_3 \cdot xH_2O$ film's surface is of utmost importance as it ensures a consistent and stable substrate for the subsequent deposition of the Cu/Bi film. Any irregularities or defects in the $WO_3 \cdot xH_2O$ film could potentially lead to inhomogeneous metal deposition, thereby affecting the overall performance and properties of the composite film structure. When a voltage of −3.0 V is applied to the working electrode, Cu/Bi nanoparticles are deposited on the $WO_3 \cdot xH_2O$ film together with the coloration of the film, which makes the device a black color. As shown in Fig. 5(b), the distribution of particle sizes and the degree of aggregation of the Cu/Bi nanoparticles are relatively large. In addition, optical scattering at the rough interface of the particles is absorbed by nearby aggregated metal particles. And these effects combined with coloration of the $WO_3 \cdot xH_2O$ film, resulting in a very low transmittance of only 0.1% for the colored RMED. It can be discerned from the energy dispersive X-ray spectroscopy (EDS) mappings depicted in Fig. 5(c-f) that within the Bi/Cu metal film obtained from the liquid electrolyte, Bi and Cu are uniformly distributed on the surface of the $WO_3 \cdot xH_2O$ film.

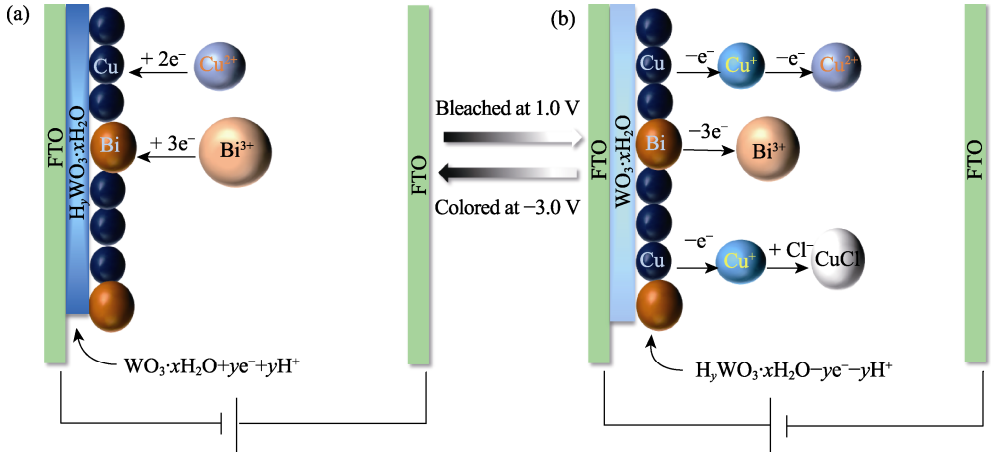

Fig. 3 Mechanisms of chemical and electrochemical reactions in the RMED during operation
(a) Colored state (metal electrodeposition); (b) Bleached state (metal stripping)

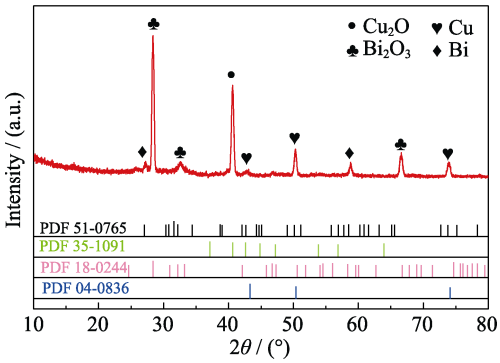

Fig. 4　GIXRD patterns of the Bi/Cu electrodeposited on the $WO_3 \cdot xH_2O$ film

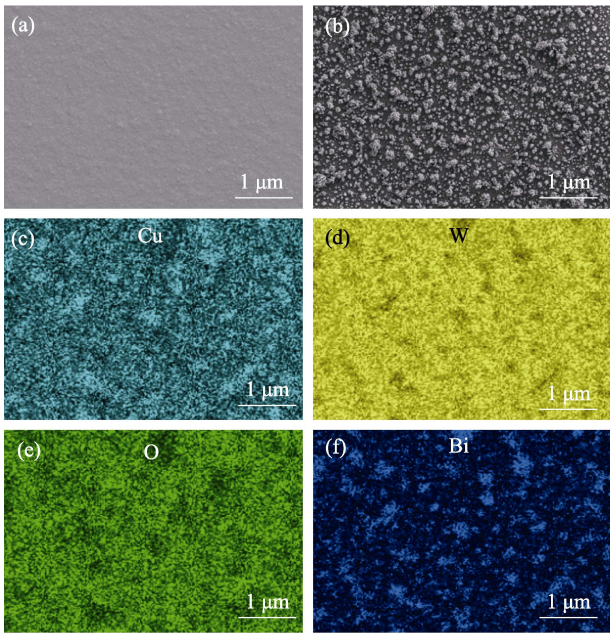

Fig. 5　SEM images and EDS mappings
(a, b) SEM images of (a) $WO_3 \cdot xH_2O$ film and (b) Bi/Cu nanoparticles; (c-f) EDS mappings of Bi/Cu nanoparticles

2.3　Electrochemical reaction kinetics

To study the electrochemical reaction kinetics at the working electrode, Fig. 6(a, b) display CV curves obtained at various scan rates ranging from –1.8 to 1.7 V. The envelope region of the CV curve corresponds to the cumulative charge storage resulting from both the diffusion-controlled process and the surface capacitance impact. Increasing the scan rate leads to a proportional increase in the envelope area of the CV curve, providing evidence of the pseudocapacitive nature. As the scan rate falls, a pair of symmetrical redox peaks progressively emerges, and the locations of the oxidation and reduction peaks steadily approach each other. This suggests that the impact of the diffusion-controlled electrochemical mechanism is strengthened when the scan rates are low. Moreover, the electrochemical kinetic mechanism of the substance can be identified by looking into the correlation between the peak current (i) and the corresponding scan rate (v):

$$i=av^b \quad (2)$$

$$\lg i=b\lg v+\lg a \quad (3)$$

where v represents the scan rate, a is a parameter that may be adjusted, and b can be determined by calculating the slope of the linear plot of $\lg i$ *vs.* $\lg v$. A Faraday process dominated by diffusion is indicated by b equal to 0.5, whereas b equal to 1.0 suggests a surface redox process that is controlled by capacitively[37]. For the purpose of this investigation, b of peaks 1 and 2 depicted in Fig. 6(c) have been determined to be 0.52 and 0.24. This substantiates that the film incorporates both electrochemical processes in the Cu/Bi ion storage rate. It is possible for the surface capacitance to contribute as much as almost 10% to the overall charge storage when the scan rate is slowed down to 10 $mV \cdot s^{-1}$ (Fig. 6(d)). The surface capacitance contribution is only around 41% when the scan rate is 100 $mV \cdot s^{-1}$, which indicates that ion diffusion plays a more significant role than surface capacitance (Fig. 6(e)). A quantitative estimate of the particular charge storage contributions to the diffusion control process and capacitance effects is presented in Fig. 6(f). The contribution connected to diffusion diminishes as the scan rate increases, and the ratio of the two components approaches equilibrium (both around 50%) at a scan rate of 100 $mV \cdot s^{-1}$. This is a natural consequence of the flow of information. As a result, the redox reaction dictated by ionic diffusion is a response that is insufficient at faster scan rates, which is comparable to the kinetics of electrochemical reactions that are described in certain literature for battery-type electrodes[38].

2.4　Electrochromic performance

The RMED has the ability to change its color between black and colorless states in a reversible manner. The related transmission spectra demonstrate a large optical modulation of 77.0% at 570 nm (Fig. 7(a)), which is greater than that of the RMED without $WO_3 \cdot xH_2O$ film (Fig. S2(a)). When a voltage of –3.0 V is applied, the ECD undergoes a transition from colorless to a black state. In this condition, the transmittance in the range of 400–1100 nm (visible-infrared band) is less than 0.03%, effectively isolating the optical transmission. Solar radiation is propagated by sunshine, with the majority of its energy being transferred mostly within the visible and infrared range (400–1100 nm).

To assess the precise manipulation of solar radiation by the RMED, the solar irradiance transmittance of the RMED in various states is calculated (Fig. 7(b)). The calculations are derived from the formula:

$$T'=\int\varphi(\lambda)T(\lambda)\mathrm{d}\lambda/\int\varphi(\lambda)\mathrm{d}\lambda \quad (4)$$

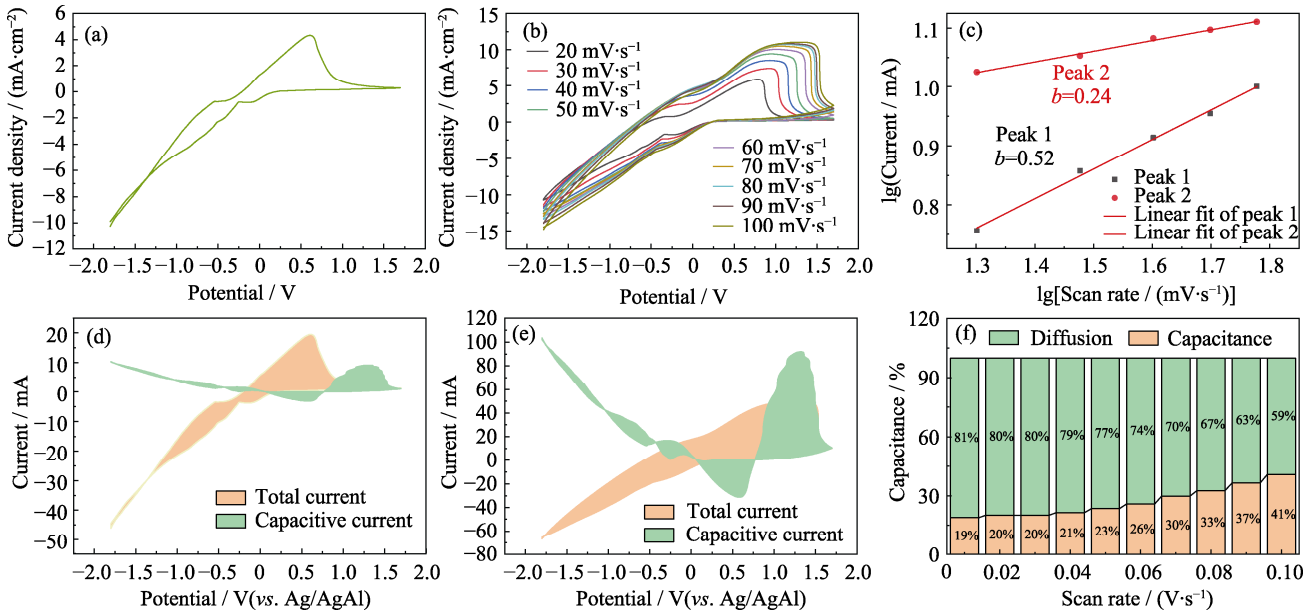

Fig. 6 Electrochemical behavior of the $WO_3 \cdot xH_2O$ film

(a) CV curve at a scan rate of 10 mV·s^{-1}; (b) CV curves at different scan rates; (c) Linear relationship between lg*i* and lg*v*; (c, d) Contribution of surface capacitance to total charge storage (shaded area) in CV curves at scan rates of (d) 10 and (e)100 mV·s^{-1}; (f) Proportion of charge storage attributed to diffusion-controlled and surface capacitance characteristics at various scan rates. Colorful figures are available on website

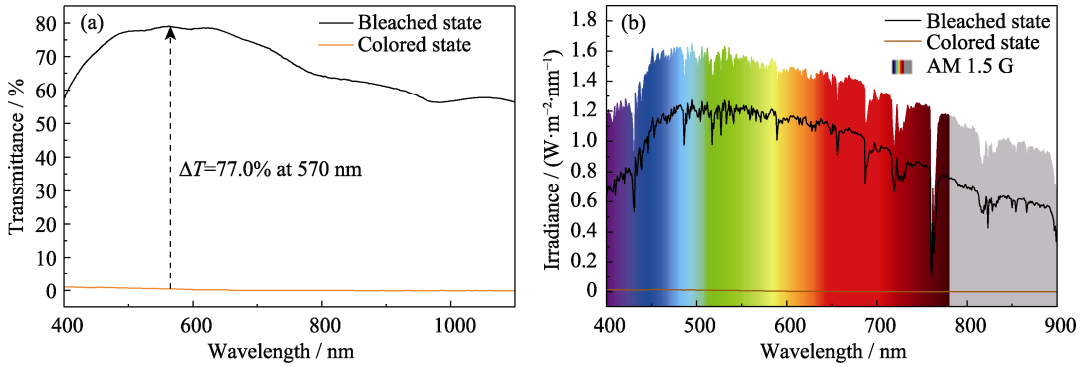

Fig. 7 Optical characteristics of the RMED

(a) Transmission spectra at the colored and bleached states measured at –3.0 and 1.0 V, respectively; (b) Solar irradiance spectra of the colored and bleached states measured at –3.0 and 1.0 V, respectively. Colorful figures are available on website

The transmittance T' is calculated by integrating the product of the transmittance $T(\lambda)$ and the solar irradiance $\varphi(\lambda)$ over the wavelength λ, divided by the integral of the solar irradiance $\varphi(\lambda)$ over the same wavelength range. The solar irradiance is measured at 1.5 air mass[39]. The RMED is capable of efficiently obstructing 99.8% of solar irradiation within the wavelength range of 400–1100 nm. This demonstrates that the RMED possesses a significant capacity for dual-band optical modulation.

As shown in Fig. 8(a), the change in transmittance of the ECD at 570 nm is examined when there was no voltage applied after the opaque state. The stability under open-circuit voltage refers to the ability of a RMED to maintain the stability of its electrode potential, electrode surface state, and optical properties when there is no external current input or output[40-41]. This stability is of crucial importance. Because in practical application scenarios, the device inevitably experiences an open-circuit state, such as during a power failure, device hibernation, or intermittent operation. If the device has poor stability under open-circuit voltage, it may lead to spontaneous oxidation or reduction of the electrode material, changes in surface morphology, degradation of optical properties, and a slowdown in color-changing response speed, which will severely affect the device's reliability, durability, and visual effect. However, a thin film is added on the surface of this RMED working electrode for modification treatment, and bromide salts are not introduced into the liquid electrolyte, which can avoid the generation of by-products and the corrosion of the deposited layer caused by excessive voltage, effectively improving the open-circuit stability of RME. As a result, the as-prepared RMED takes 225.0 s to fully return to transparency when there is no power supply.

The duration required for the transmittance to reach 90% of its maximum change during the coloration process is termed coloration time (t_c). Conversely, the period needed for it to revert to its original state is referred to as bleaching time (t_b). The response times of RMED are determined by analyzing real-time transmission spectra obtained while subjecting the system to periodic potentials of –3.0 V (for coloration) and 1.0 V (for bleaching). The measured response times are 15.8 s for coloration and 16.2 s for bleaching (Fig. 8(b)), representing a significant improvement compared to RMED without $WO_3 \cdot xH_2O$ film (Fig. S2(b)) and over previous RMEDs[11-13]. By simultaneously recording the changes of current and transmittance at a certain wavelength during the coloration process, the coloration efficiency (CE) of the ECD is obtained, which is an important evaluation index of ECDs. The CE characterizes the ability of a device to change color per unit charge and can be calculated by the formula:

$$CE=\Delta OD/(Q/A) \quad (5)$$

$$\Delta OD=\lg(T_b/T_c) \quad (6)$$

where ΔOD is the change in optical density, T_b and T_c are the transmittance of the bleached and colored states of the ECD respectively, and Q/A is the injected charge Q per unit electrode area A. The CE of the ECD tested at a wavelength of 570 nm is determined to be 17.1 $cm^2 \cdot C^{-1}$, as shown in Fig. 8(c). The overall CE of the RMED is quite poor when compared to other well-established ECDs that utilize metal compounds and organic compounds. This device follows this trend and also exhibits a low CE. Fig. 8(d) illustrates the alteration in transmittance throughout the successive processes of bleaching and coloration in the RMED. It was achieved by applying square wave voltages of –3.0 V for 30 s and 1.0 V for 40 s. The as-prepared RMED exhibits excellent cyclic stability, maintaining 96.6% of the original optical modulation after 60000 s.

When the device is in the colored state, it can effectively absorb and reflect the heat part of the solar radiation, reducing the transfer of heat to the other side, thus achieving the heat insulation function[42]. In order to determine whether the manufactured device affects the internal temperature change and can act as an actual window, a 3 cm× 4 cm RMED was attached to a model house. An infrared lamp was used to simulate the spectrum and intensity of sunlight, and the RMED was placed between the infrared lamp and a heat sensor, as shown in Fig. 9(a). The heat sensor was used to measure the temperature change on the other side of the device. Firstly, the temperature rises of the device in the state of soda-lime glass and in the transparent state (without the electrodeposition heat insulation operation) were recorded. Then, the device was made to enter the colored

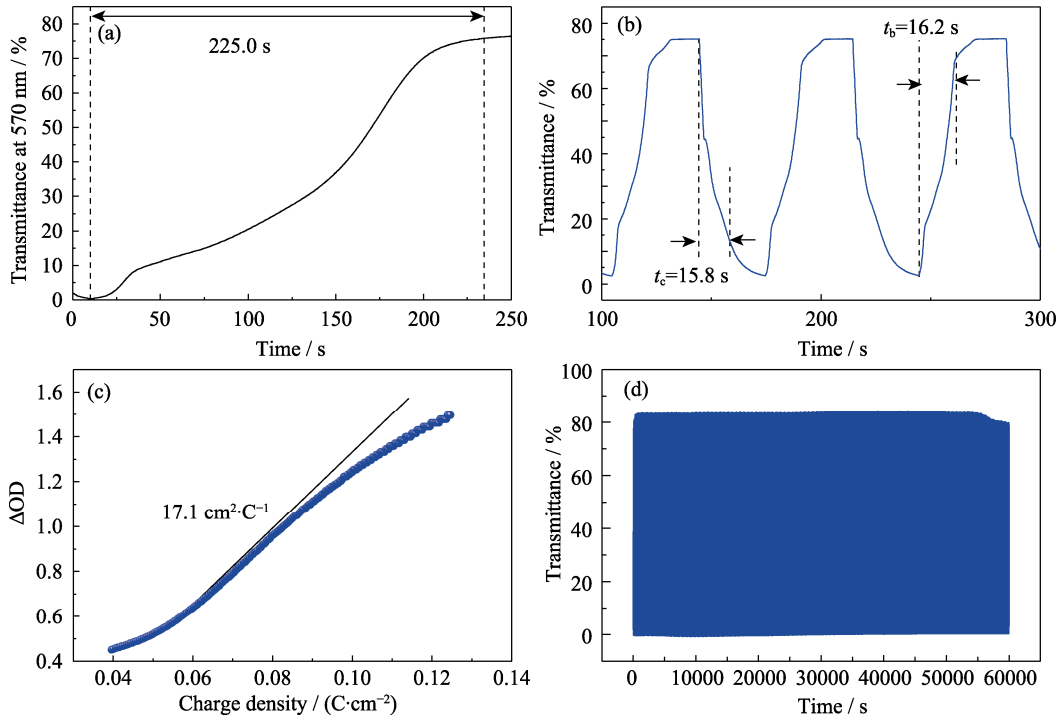

Fig. 8　Electrochemical and EC properties of the RMED

(a) Duration needed for the RMED to go from coloration to bleaching at a wavelength of 570 nm when operating at open circuit voltage; (b) Real-time transmittance curve of the RMED recorded at 570 nm by applying a square wave potential of –3.0 V for 30 s and 1.0 V for 40 s; (c) Optical density variations with respect to charge density; (d) Cyclic performance of the RMED measured by applying –3.0 V for 30 s and 1.0 V for 40 s

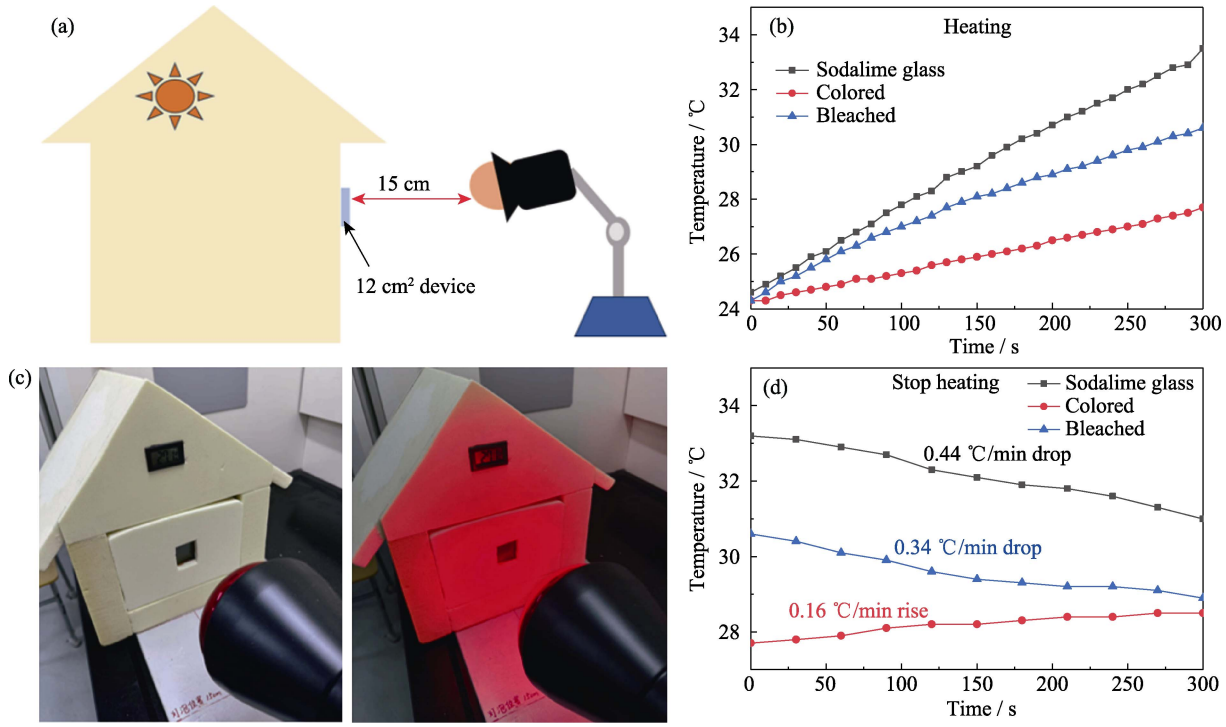

Fig. 9 Infrared blocking performance of the RMED smart window in a model house

(a) Schematic diagram of the indoor temperature change experiment using the model house; (b) Indoor temperature change curves of each mode during heating process of the house; (c) Physical pictures of the house during heating and heating-stopping simulation; (d) Indoor temperature change curves of each mode during the heating-stopping process

heat-insulating state, and the temperature change was recorded again. After heating the house model with infrared lamps for 300 s, the temperature changes inside the house model during heating and after heating were recorded, as shown in Fig. 9(b-d). When sodalime glass was used to simulate ordinary windows, the initial indoor temperature was 24.6 ℃. After being irradiated by the infrared lamp for 300 s, the temperature rose to 33.2 ℃, and it dropped to 31.0 ℃ after the heating was stopped for 5 min. When the bleached state of the RMED functioned as the windows of the house model, the initial indoor temperature was 24.4 ℃. After being irradiated by the infrared lamp for 300 s, the temperature rose to 30.6 ℃, and it dropped to 28.9 ℃ after the heating was stopped for 5 min. When the colored state of RMED functioned as the windows of the house model, the initial indoor temperature was 24.3 ℃. After being irradiated by the infrared lamp for 300 s, the temperature rose to 27.7 ℃, and it rose to 28.5 ℃ after the heating was stopped for 5 min. It indicates that the black metal film in the colored state of the RMED has absorbed most of the solar radiation. Therefore, the as-prepared RMED with strong heat insulation ability can effectively reduce the dependence of buildings on air-conditioning systems in summer, thus becoming an excellent candidate for EC smart windows.

3 Conclusions

In summary, an ECD combining RME and the $WO_3 \cdot xH_2O$ film has been successfully fabricated. By depositing Cu/Bi metals on electrodeposited $WO_3 \cdot xH_2O$ film, the RMED exhibits a black state with a near-zero transmittance in the wavelength range of 400–1100 nm, and it achieves a large optical modulation of 77.0% at 570 nm. Furthermore, it maintains 96.6% of the initial optical modulation after cycling for 60000 s. The RMED has a coloration time of 15.8 s and a bleaching time of 16.2 s. It has relatively high stability under open-circuit voltage and also possesses excellent heat insulation performance. The results have shown that the integration of traditional EC materials with metal electrodeposition expands the possibilities of EC technology for applications in smart windows and electronic displays.

Supporting materials

Supporting materials related to this article can be found at https://doi.org/10.15541/jim20250017.

References:

[1] KHANDEKAR M L, MURTY T S, CHITTIBABU P. The global warming debate: a review of the state of science. *Pure Appl.*

Geophys., 2005, **162(8/9):** 1557.
[2] GRANQVIST C G. Transparent conductors as solar energy materials: a panoramic review. *Sol. Energy Mater. Sol. Cells*, 2007, **91(15):** 1529.
[3] SUMBOJA A, LIU J M, ZHENG W G, *et al*. Electrochemical energy storage devices for wearable technology: a rationale for materials selection and cell design. *Chem. Soc. Rev.*, 2018, **47(15):** 5919.
[4] KIM H, SON M, AHN S H, *et al*. Comparison of electrochromic characteristics of electrochromic device upon various sintering methods of Sol-Gel based WO_3 electrode. *Curr. Appl. Phys.*, 2020, **20(6):** 782.
[5] EH A L S, TAN A W M, CHENG X, *et al*. Recent advances in flexible electrochromic devices: prerequisites, challenges, and prospects. *Energy Technol.*, 2018, **6(1):** 33.
[6] ZHANG R C, ZHANG Z B, HAN J C, *et al*. Advanced liquid crystal-based switchable optical devices for light protection applications: principles and strategies. *Light Sci. Appl.*, 2023, **12(1):** 11.
[7] GLOGIC E, FUTSCH R, THENOT V, *et al*. Development of eco-efficient smart electronics for anticounterfeiting and shock detection based on printable inks. *ACS Sustain. Chem. Eng.*, 2021, **9(35):** 11691.
[8] WANG J L, LIU J W, SHENG S Z, *et al*. Manipulating nanowire assemblies toward multicolor transparent electrochromic device. *Nano Lett.*, 2021, **21(21):** 9203.
[9] ALCARAZ G K A, JUAREZ-ROLON J S, BURPEE N A, *et al*. Thermally-stable dynamic windows based on reversible metal electrodeposition from aqueous electrolytes. *J. Mater. Chem. C*, 2018, **6(8):** 2132.
[10] ARAKI S, NAKAMURA K, KOBAYASHI K, *et al*. Electrochemical optical-modulation device with reversible transformation between transparent, mirror, and black. *Adv. Mater.*, 2012, **24(23):** 122.
[11] EH A L S, CHEN J, ZHOU X, *et al*. Robust trioptical-state electrochromic energy storage device enabled by reversible metal electrodeposition. *ACS Energy Lett.*, 2021, **6(12):** 4328.
[12] ZIEGLER J P. Status of reversible electrodeposition electrochromic devices. *Sol. Energy Mater. Sol. Cells*, 1999, **56(3/4):** 477.
[13] LAIK B, CARRIÈRE D, TARASCON J M. Reversible electrochromic system based on aqueous solution containing silver. *Electrochim. Acta*, 2001, **46(13/14):** 2203.
[14] BARILE C J, SLOTCAVAGE D J, HOU J Y, *et al*. Dynamic windows with neutral color, high contrast, and excellent durability using reversible metal electrodeposition. *Joule*, 2017, **1(1):** 133.
[15] BARILE C J. Electrolyte dynamics in reversible metal electrodeposition for dynamic windows. *J. Appl. Electrochem.*, 2018, **48(4):** 443.
[16] HOWARD B M, ZIEGLER J P. Optical properties of reversible electrodeposition electrochromic materials. *Sol. Energy Mater. Sol. Cells*, 1995, **39(2/3/4):** 309.
[17] ISLAM S M, FINI C N, BARILE C J. Dynamic windows based on reversible metal electrodeposition with enhanced functionality. *J. Electrochem. Soc.*, 2019, **166(8):** D333.
[18] JEONG K R, LEE I, PARK J Y, *et al*. Enhanced black state induced by spatial silver nanoparticles in an electrochromic device. *NPG Asia Mater.*, 2017, **9:** e362.
[19] LUO G, SHEN L Y, ZHENG J M, *et al*. A europium ion doped WO_3 film with the bi-functionality of enhanced electrochromic switching and tunable red emission. *J. Mater. Chem. C*, 2017, **5(14):** 3488.
[20] DOV N E, SHANKAR S, COHEN D, *et al*. Electrochromic metallo-organic nanoscale films: fabrication, color range, and devices. *J. Am. Chem. Soc.*, 2017, **139(33):** 11471.
[21] ASSIS L M N, LEONES R, KANICKI J, *et al*. Prussian blue for electrochromic devices. *J. Electroanal. Chem.*, 2016, **777:** 33.
[22] ZHI M Y, HUANG W X, SHI Q W, *et al*. Enhanced electrochromic performance of vanadium pentoxide/reduced graphene oxide nanocomposite film prepared by the Sol-Gel method. *J. Electrochem. Soc.*, 2016, **163(10):** H891.
[23] QIU M J, SUN P, ZHANG B, *et al*. Reliable information encryption and digital display applications based on multistate smart windows. *Adv. Opt. Mater.*, 2018, **6(22):** 1800338.
[24] SUI C X, PU J K, CHEN T H, *et al*. Dynamic electrochromism for all-season radiative thermoregulation. *Nat. Sustain.*, 2023, **6(4):** 428.
[25] JIA Z F, SUI Y M, QIAN L, *et al*. Electrochromic windows with fast response and wide dynamic range for visible-light modulation without traditional electrodes. *Nat. Commun.*, 2024, **15(1):** 6110.
[26] ZHANG Y X, XU B, HUANG B K, *et al*. Color-neutral smart window enabled by gradient reversible alloy deposition. *ACS Energy Lett.*, 2024, **9(8):** 4162.
[27] NGUYEN T V, DO H, GUO W W, *et al*. Tungsten oxide-modified ITO electrode for electrochromic window based on reversible metal electrodeposition. *Electron. Mater. Lett.*, 2022, **18(1):** 36.
[28] SHENG K, XUE B, ZHENG J M, *et al*. A transparent to opaque electrochromic device using reversible Ag deposition on PProDOT-Me_2 with robust stability. *Adv. Opt. Mater.*, 2021, **9(11):** 2002149.
[29] ZHANG X Q, SUI Y M, YEASMIN S, *et al*. Fast-switching electrochromic device enabled by Fe^{2+}-mediated MnO_2/Mn^{2+} redox reactions. *ACS Appl. Electron. Mater.*, 2024, **6(11):** 8163.
[30] EVANS R C, AUSTIN R, MILLER R C, *et al*. Surface-facet-dependent electrochromic properties of WO_3 nanorod thin films: implications for smart windows. *ACS Appl. Nano Mater.*, 2021, **4(4):** 3750.
[31] LI Y Q, MCMASTER W A, WEI H, *et al*. Enhanced electrochromic properties of WO_3 nanotree-like structures synthesized *via* a two-step solvothermal process showing promise for electrochromic window application. *ACS Appl. Nano Mater.*, 2018, **1(6):** 2552.
[32] ZHOU Z Q, CHEN Z, MA D Y, *et al*. Porous $WO_3 \cdot 2H_2O$ film with large optical modulation and high coloration efficiency for electrochromic smart window. *Sol. Energy Mater. Sol. Cells*, 2023, **253:** 112226.
[33] ISLAM S M, HERNANDEZ T S, MCGEHEE M D, *et al*. Hybrid dynamic windows using reversible metal electrodeposition and ion insertion. *Nat. Energy*, 2019, **4(3):** 223.
[34] HERNANDEZ T S, BARILE C J, STRAND M T, *et al*. Bistable black electrochromic windows based on the reversible metal electrodeposition of Bi and Cu. *ACS Energy Lett.*, 2018, **3(1):** 104.
[35] EH A L S, LIN M F, CUI M Q, *et al*. A copper based reversible electrochemical mirror device with switchability between transparent, blue, and mirror states. *J. Mater. Chem. C*, 2017, **5(26):** 6547.
[36] GUPTA S, SINGH R, ANOOP M D, *et al*. Electrochemical sensor for detection of mercury (II) ions in water using nanostructured bismuth hexagons. *Appl. Phys. A*, 2018, **124(11):** 737.
[37] ZHANG C, LI S, WU R, *et al*. Robust MnO_2-WO_3 complementary electrochromic device enabled by reversible electrodeposition of MnO_2. *Nano Lett.*, 2024 **24(51):** 16360.
[38] YUAN Y L, LU Y D, JIA B E, *et al*. Integrated system of solar cells with hierarchical $NiCo_2O_4$ battery-supercapacitor hybrid devices for self-driving optical-emitting diodes. *Nano-Micro Lett.*, 2019, **11(1):** 42.
[39] SUN J W, WAN X Y, YANG T, *et al*. High-performance tungsten-niobium bimetallic oxide films with designable electrochromic properties. *Sol. Energy Mater. Sol. Cells*, 2023, **256:** 112318.
[40] CHO S M, KIM S, KIM T Y, *et al*. New switchable mirror device with a counter electrode based on reversible electrodeposition. *Sol. Energy Mater. Sol. Cells*, 2018, **179:** 161.
[41] TAO X, LIU D Q, LIU T W, *et al*. A bistable variable infrared emissivity device based on reversible silver electrodeposition. *Adv. Funct. Mater.*, 2022, **32(32):** 2202661.
[42] PENG Y C, FAN L L, JIN W L, *et al*. Coloured low-emissivity films for building envelopes for year-round energy savings. *Nat. Sustain.*, 2021, **5(4):** 339.

基于 $WO_3 \cdot xH_2O$ 与可逆金属电沉积的无色/黑色转换电致变色器件

宛心怡[1], 王文奇[1], 李加诚[1], 赵俊亮[2], 马董云[1], 王金敏[1]

(1. 上海理工大学 材料与化学学院, 上海 200093; 2. 上海半人马企业发展集团有限公司, 上海 201306)

摘 要: 可逆金属电沉积器件(Reversible Metal Electrodeposition Device, RMED)的电致变色(Electrochromic, EC)智能窗为动态调节光和热的传输提供了一个极具吸引力的替代方案。本工作通过在氟掺杂氧化锡(Fluorine-doped Tin Oxide, FTO)透明导电玻璃上电沉积 $WO_3 \cdot xH_2O$ 薄膜, 再利用 Bi/Cu 的可逆金属电沉积来构建电致变色器件(Electrochromic Device, ECD)。电解质由 $CuCl_2$、$BiCl_3$、KCl 和 HCl 水溶液组成, 为电化学过程和电沉积过程提供必要的成分。该器件可在无色和黑色状态之间快速转换, 在 570 nm 波长处实现了 77.0%的光调制幅度。在黑色状态下, ECD 在 400~1100 nm 范围内呈现出接近零的透过率。此外, 经历 60000 s 的着色/褪色循环后, 该器件能够维持其初始光调制幅度的 96.6%, 展现出良好的循环稳定性。所制备的 RMED 在开路电压下具有相对较高的稳定性, 还拥有出色的隔热性能。这些研究结果为克服 RMED 循环稳定性差以及提高 ECD 的光调制幅度提供了一种解决方案。

关 键 词: 可逆金属电沉积; 电致变色; $WO_3 \cdot xH_2O$

中图分类号: TQ174 **文献标志码:** A **文章编号:** 1000-324X(2025)10-1163-10

Supporting Materials:

Colorless/Black Switching Electrochromic Device Based on $WO_3 \cdot xH_2O$ and Reversible Metal Electrodeposition

WAN Xinyi[1], WANG Wenqi[1], LI Jiacheng[1], ZHAO Junliang[2], MA Dongyun[1], WANG Jinmin[1]

(1. School of Materials and Chemistry, University of Shanghai for Science and Technology, Shanghai 200093, China; 2. Shanghai Berma Enterprise Development Group Co., Ltd., Shanghai 201306, China)

A series of devices were fabricated. All these devices had a thin film and were placed in an electrolyte environment. Their uniqueness lies in the different atomic ratios of Cu to Bi within each device. To gain an in-depth understanding of the performance of these devices, we conducted a comprehensive test on their response times (Fig. S1). When the atomic ratio of Cu to Bi is 5 : 1 and 4 : 1, respectively, a coloration voltage of –3 V is applied to the RMED for 30 s to make it colored. Then, a bleaching voltage of 1 V is applied for 100 s for the bleaching process. When the atomic ratio of Cu to Bi is 2 : 1, 1 : 1, 1 : 2 and 1 : 3, respectively, a coloration voltage of –3 V is applied to the RMED for 30 s to make it colored. Then, a bleaching voltage of 1 V is applied for 40 s to carry out the bleaching process.

Without adding a thin film, using FTO as both the working electrode and counter electrode, and keeping the electrolyte concentration unchanged, a device was fabricated. Then, the optical modulation and response time of this device were tested (Fig. S2). Due to the

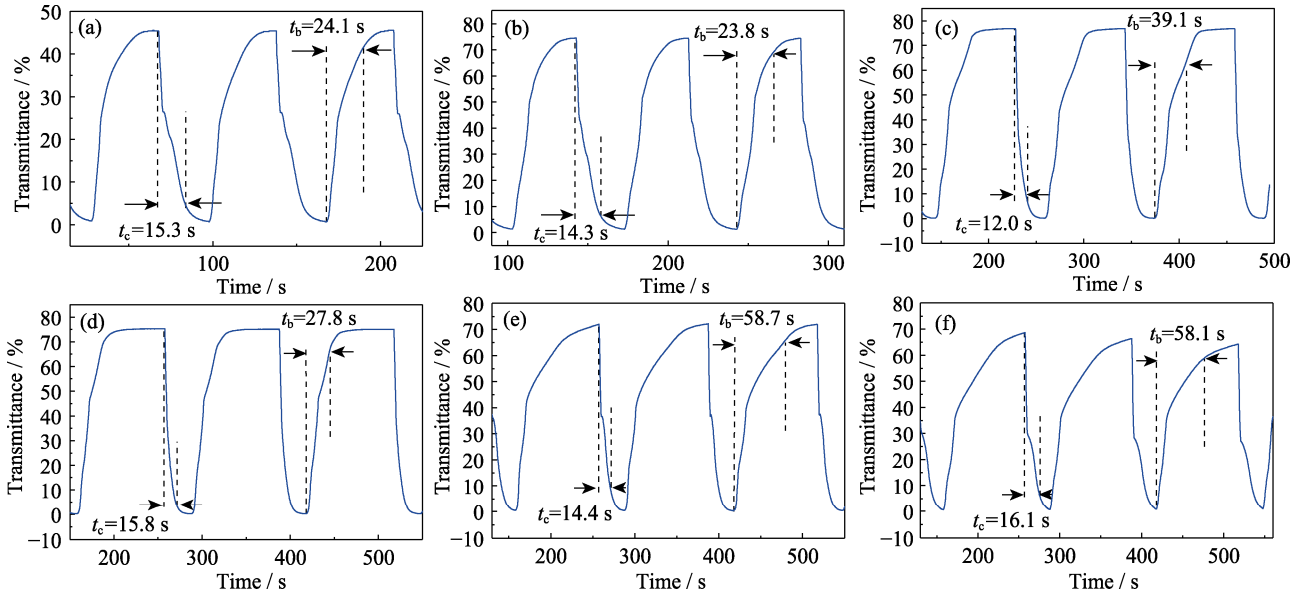

Fig. S1　Real-time transmittance curves at 570 nm for RMEDs with different metal atomic ratios under coloration (–3.0 V) and bleaching (1.0 V) conditions

(a) Cu:Bi = 5 : 1; (b) Cu:Bi = 4 : 1; (c) Cu:Bi = 2 : 1; (d) Cu:Bi = 1 : 1; (e) Cu:Bi = 1 : 2; (f) Cu:Bi = 1 : 3

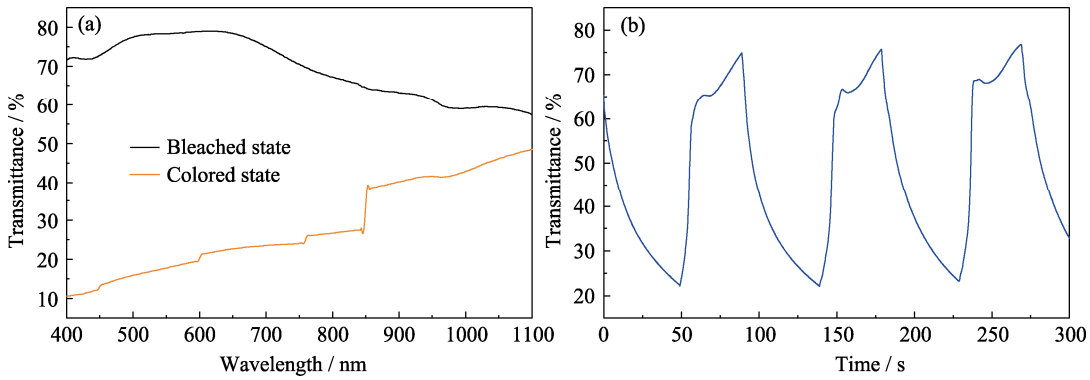

Fig. S2　Electrochromic properties of the RMED without $WO_3 \cdot xH_2O$ film

(a) Transmission spectra in the colored (–3.0 V for 30 s) and bleached (1.0 V for 40 s) states; (b) Real-time transmittance curve at 570 nm

self-fading phenomenon of the RMED, continuous power supply is required when the transmittance of the colored state is tested. In addition, a voltage of –3 V is applied for 30 s before the start of the experiment. If the $WO_3 \cdot xH_2O$ film is not used in the device, the structure of the RMED will change, and the optical modulation and response times of the device will be significantly degraded. This also proves that adding the $WO_3 \cdot xH_2O$ film will greatly improve the performance of the device.